

# Magnetoelastic effects in doped Fe<sub>2</sub>P

Z. Gercsi,<sup>1</sup> E. K. Delczeg-Czirjak,<sup>2</sup> L. Vitos,<sup>3</sup> A. S. Wills,<sup>4</sup> A. Daoud-Aladine,<sup>5</sup> and K.G. Sandeman<sup>1</sup>

<sup>1</sup>*Dept. of Physics, Blackett Laboratory, Imperial College London, London SW7 2AZ, United Kingdom*

<sup>2</sup>*Division of Materials Theory, Department of Physics and Astronomy,  
Uppsala University, Box 516, SE 751210 Uppsala, Sweden*

<sup>3</sup>*Applied Materials Physics, Department of Materials Science and Engineering,  
Royal Institute of Technology, SE-100 44 Stockholm, Sweden*

<sup>4</sup>*Department of Chemistry, University College London,  
20 Gordon Street, London WC1H 0AJ, United Kingdom*

<sup>5</sup>*ISIS facility, Rutherford Appleton Laboratory, Chilton,  
Didcot, Oxfordshire, OX11 0QX, United Kingdom*

We use combine high resolution neutron diffraction (HRPD) with density functional theory (DFT) to investigate the exchange striction mechanism at the Curie temperature ( $T_C$ ) of Fe<sub>2</sub>P and to examine the effect of boron and carbon doping on the P site. We find a significant contraction of the basal plane on heating through  $T_C$  with a simultaneous increase of the  $c$ -axis that results in a small overall volume change of  $\sim 0.01\%$ . At the magnetic transition the Fe<sub>I</sub>-Fe<sub>I</sub> distance drops significantly and becomes shorter than Fe<sub>I</sub>-Fe<sub>II</sub>. The shortest metal-metalloid (Fe<sub>I</sub>-P<sub>I</sub>) distance also decreases sharply. Our DFT model reveals the importance of the latter as this structural change causes a redistribution of the Fe<sub>I</sub> moment along the  $c$ -axis (Fe-P chain). We are able to understand the site preference of the dopants, the effect of which can be linked to the increased moment on the Fe<sub>I</sub>-site, triggered by both valence electron and structural contributions.

PACS numbers: 75.30.Sg, 75.30.Kz, 75.80.+q, 75.30.Et

## I. INTRODUCTION

Fe<sub>2</sub>P-based magnetic alloys attract interest from many areas of physics, materials science and geophysics research. They are found in meteorites and are considered as a candidate minor phase present in the Earth's core<sup>1,2</sup>. An understanding of the mechanism of formation of these minerals can help to identify the histories of planetary bodies and the composition of the Earth's outer core. In LiFePO<sub>4</sub>-based battery materials, a percolating nano-network of metal-rich phosphides including Fe<sub>2</sub>P can significantly enhance electrical conductivity<sup>3</sup>. Fe<sub>2</sub>P-based alloys can furthermore be prepared as 1-dimensional (1D) nanowires and nanocables<sup>4</sup>. Of most relevance to this article, however, is the prospect of hexagonal Fe<sub>2</sub>P-based alloys being used as room temperature magnetic refrigerants.

Fe<sub>2</sub>P exhibits a first order magnetic transition from a ferromagnetic (FM) state to a paramagnetic one (PM) at 217 K<sup>5</sup> accompanied by a significant change in the  $c/a$ -ratio of the hexagonal structure. The magnetisation deviates from the Curie-Weiss law for temperatures up to 700 K and net magnetism can be observed above the Curie temperature in fields of only a few Tesla. In nanocable form, the magnetic transition temperature is shifted 10-50 K higher compared to the parent composition because of strong strain and/or carbon doping<sup>4</sup>. The increase in the Curie temperature,  $T_C$  with only a small, partial replacement of phosphorus with other  $p$ -block elements (B, Si or As) is remarkable. 10% replacement of P by B leads to  $\sim 120\%$  change, while the same amount of Si and As substitution also results in a  $\sim 70\%$  and  $\sim 60\%$  increase (Fig. 1) respectively, with a simultaneous change

in the nature of the transition from first order to second order<sup>6-8</sup>. Such large changes in  $T_C$  are not restricted to doping by  $p$ -block elements. Partial replacement of Fe by Mn results in a significant increase of the saturation magnetisation, while the first order nature of the metamagnetic transition is preserved up to and beyond room temperature and is tuned by magnetic field at a rate of  $\sim 3 \text{ K T}^{-1}$ <sup>9,10</sup>.

The metamagnetism of Fe<sub>2</sub>P shares many features with the itinerant electron metamagnetism (IEM) of La(Fe,Si)<sub>13</sub><sup>11</sup>. That material also has a PM to FM transition, the temperature of which can be tuned from around 190 K to well above 300 K. The high magnetisation state can be induced by a magnetic field above  $T_C$ , and the metamagnetic transition is tuned by field at a rate of around  $4 \text{ K T}^{-1}$ . As in Fe<sub>2</sub>P the first or second order nature of its metamagnetism depends on the substituent (e.g. Co or Mn) or intercalating atom (e.g. H or C)<sup>12,13</sup>. Fe<sub>2</sub>P-based and La(Fe,Si)<sub>13</sub>-based alloys are two of the leading contenders for scale-up as magnetic refrigerants, due to their tunable metamagnetism, their large room temperature magnetocaloric effect (MCE) and the fact that they are mostly composed of abundantly available  $3d$  and  $p$ -block elements<sup>14</sup>.

There has been a recent growth in theoretical investigations of the origin and tuneability of metamagnetism in Fe<sub>2</sub>P and of the appearance of a body centered orthorhombic structure in substituted alloys. This is partly motivated by the sensitivity to doping of the Curie temperature and any associated thermomagnetic hysteresis, and given added impetus more recently by the investigation of the MCE of industrially-scaled quantities of material where good compositional tolerance is re-

quired. A Landau-Ginzburg free energy analysis based on fixed-spin-moment (FSM) calculations that took into account the effect of spin fluctuations revealed the metamagnetic nature of the Fe-atoms at a particular crystallographic (3f) site in the parent alloy as well as in the doped counterparts<sup>15,16</sup>. Using linear muffin tin orbitals in the atomic sphere approximation (ASA), Severin et al.<sup>17</sup> found that the magnetic moments in the inter-related hexagonal and orthorhombic structures are very similar and scale with the nearest-neighbour Fe-P distances. We recently found that the phonon vibrational free energy stabilizes the hexagonal phase, whereas the electronic and magnetic entropies favour a low symmetry orthorhombic structure in Si-substituted  $\text{Fe}_2\text{P}_{1-x}\text{Si}_x$  alloys<sup>18</sup>. An analysis of the exchange constants in the hexagonal structure of B-, Si- and As-doped  $\text{Fe}_2\text{P}$  helps to explain trends in Curie temperature. A principal interlayer Fe-Fe interaction was identified as controlling the strength of ferromagnetism<sup>19</sup>.

In the present paper we employ a joint experimental-theoretical approach that we have used elsewhere to uncover the microscopic mechanism of metamagnetism in Mn-based antiferromagnets. By using density functional theory (DFT) in combination with structural information from high resolution neutron diffraction (HRPD)<sup>20</sup> we have previously mapped the magnetic phase diagram of Mn-based metallic orthorhombic compounds in the  $Pnma$  space group as a function of Mn-Mn distance<sup>21</sup> and have predicted new antiferromagnetic metamagnets<sup>22,23</sup>. Taking the same approach here, we first analyse and compare the peculiar magnetoelastic coupling of the metamagnetic transition in  $\text{Fe}_2\text{P}$ , in boron-doped  $\text{Fe}_2(\text{P},\text{B})$  and, for the first time, carbon-doped  $\text{Fe}_2(\text{P},\text{C})$  using HRPD. In the second part of the article, we use a simple DFT model to further interpret the large interatomic changes at the magnetic transition. Our aim is to provide clues as to how to control and optimise the structure-magnetism relationship in this highly tuneable materials class.

## II. PREVIOUS EXPERIMENTAL FINDINGS

$\text{Fe}_2\text{P}$  is the prototype structure of the hexagonal space group 189 ( $P\bar{6}2m$ ) with 9 atoms in the unit cell. The 6 Fe atoms occupy two non-equivalent threefold symmetry sites (3f and 3g), while the phosphorus atoms sit on a singlefold (1b) and on a twofold position (2c) in the crystal lattice. Here we adopt the following established notation:  $\text{Fe}_I$  for the 3f ( $x_I, 0, 0$ ) positions,  $\text{Fe}_{II}$  for the 3g ( $x_{II}, 0, 1/2$ ) positions, and  $\text{P}_I$  and  $\text{P}_{II}$  for the 2c ( $1/3, 2/3, 0$ ) and 1b ( $0, 0, 1/2$ ) positions of the P atoms, respectively. The hexagonal cell is composed of triangles in the  $ab$  plane as shown in Figure 2. The iron atoms that alternate along the  $c$ -axis are surrounded either by four P-atoms with tetrahedral symmetry ( $\text{Fe}_I$ ) or by five P-atoms forming a pyramid ( $\text{Fe}_{II}$ ). It was reported previously<sup>24</sup> that the  $c$ -axis lattice parameter increases with temperature while the  $a$ - and  $b$ -axes (basal plane)

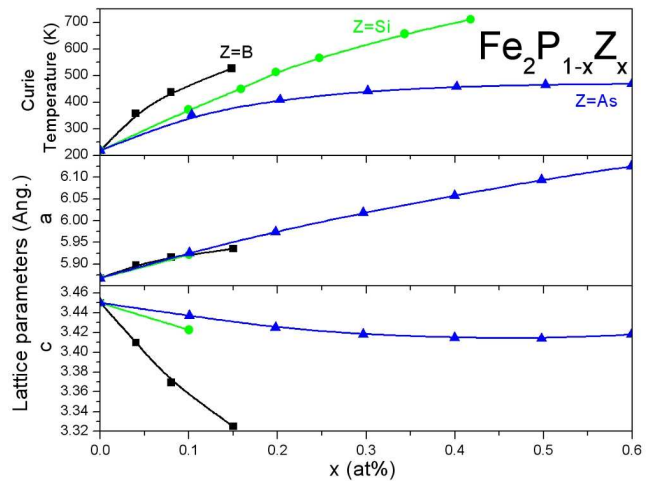


Figure 1: (Color online) The effect of boron, silicon and arsenic doping in  $\text{Fe}_2\text{P}_{1-x}\text{Z}_x$  on the magnetic ordering temperature  $T_C$  (top) and the room temperature lattice parameters (bottom)<sup>6-8</sup>.

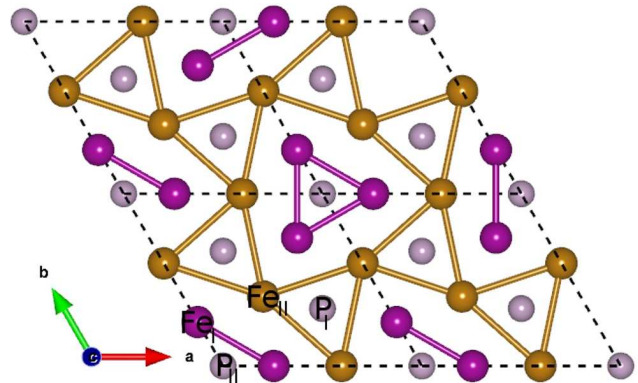


Figure 2: (Color online) Atomic arrangement of the  $\text{Fe}_2\text{P}$  in the basal plane. Fe atoms occupy two non-equivalent threefold symmetry sites, 3f ( $\text{Fe}_I$ ) and 3g ( $\text{Fe}_{II}$ ), and the phosphorus atoms sit on a single-fold 1b ( $\text{P}_I$ ) and two-fold position, 2c ( $\text{P}_{II}$ ) in the hexagonal crystal lattice.  $\text{Fe}_I$  ( $x_I, 0, 0$ ) atoms share the same plane with  $\text{P}_I$  ( $1/3, 2/3, 0$ ) and  $\text{Fe}_{II}$  atoms ( $x_{II}, 0, 1/2$ ) with  $\text{P}_{II}$  ( $0, 0, 1/2$ ), respectively.

exhibit negative thermal expansion. The same authors used a strain gauge dilatometer to measure the linear thermal expansion ( $\Delta l/l$ ) of a single crystal of  $\text{Fe}_2\text{P}$  upon cooling through the first order type magnetic transition and found a sharp increase of  $\frac{\Delta a}{a} = 0.74 \times 10^{-3}$  with the simultaneous decrease of the  $c$ -axis: ( $\frac{\Delta c}{c} = -0.84 \times 10^{-3}$ ).

The coupling between the structure and magnetism is further manifested by the effect of doping shown in Fig. 1. A significant increase in Curie temperature upon partial replacement of the P atoms by other  $p$ -block elements such as B, Si and As has been observed.<sup>6-8</sup> Catalano et al.<sup>6</sup> investigated the effect of isovalent substitution of As for P on the crystalline lattice and on magnetic proper-

ties. The authors found that the larger atomic radius As can be continuously accommodated into the hexagonal lattice between  $0 \leq x \leq 0.65$  in  $\text{Fe}_2\text{P}_{1-x}\text{As}_x$  with a strong site preference for the  $\text{P}_I$  (2c) position. The monotonic increase of the lattice volume with As addition is a compromise of a moderate increase of  $a$ -axis and a simultaneous contraction of the lattice along the  $c$ -direction. The same tendency was observed by the substitution of larger atomic radius, non-isovalent Si for P by Jernberg et al.<sup>8</sup> Interestingly, Si atoms were also found to show some site preference for the  $\text{P}_I$  position with opposing trends in the  $a$  and  $c$  lattice parameters and a significant increase in the magnetic ordering temperature. Silicon addition above  $x \leq 0.1$  results in a change from the hexagonal lattice structure into one with a body-centered orthorhombic,  $\text{Imm}2$  (44) symmetry.

Finally, the partial replacement of P by the substantially smaller atomic radius boron results in a formidable increase of the Curie temperature. The solid solubility of the B atoms in  $\text{Fe}_2\text{P}_{1-x}\text{B}_x$  is, however, limited to  $x \approx 0.15$  due to the formation of other  $\text{Fe}_5\text{PB}_2$ ,  $\text{Fe}_3\text{B}$  and  $\text{Fe}_2\text{B}$  refractory borides at higher B concentrations. Chandra et al. established by means of Mössbauer spectroscopy that the small boron atoms, unlike the larger elements (As and Si), occupy the  $\text{P}_{II}$  (1b) singlefold position in the hexagonal lattice<sup>7</sup>. Another consequence of the chemical pressure on the hexagonal lattice caused by boron addition as compared to the parent alloy or to the Si/As-doped compositions is decreased lattice volume. Despite such differences, the monotonic increase of the  $a$  and decrease of the  $c$  lattice parameters of the unit cell is strikingly similar to the effect of larger  $p$ -element dopants (Fig. 1). An additional consequence of boron doping is that the first-order PM-FM transition of undoped  $\text{Fe}_2\text{P}$  becomes second order.

### III. METHODS

#### A. Experimental Methods

The samples used in this study were prepared from ultra high purity elements. The powders were mixed to weight ratios to according to nominal compositions of  $\text{Fe}_2\text{P}$  and  $\text{Fe}_2\text{P}_{0.96}\text{Z}_{0.04}$ , ( $\text{Z}=\text{B}$  or  $\text{C}$ ) and then thoroughly ground together in an agate mortar under protective atmosphere. The initial powders were then pressed into pellets and sealed into quartz ampoules under protective argon atmosphere for solid state reaction. The initial annealing temperature was raised slowly ( $0.5 \text{ K min}^{-1}$ ) up to 673 K, where each sample was kept for 4 hours for an initial reaction. There was a subsequent heating step (at  $1 \text{ K min}^{-1}$ ) up to 1273 K where the temperature was held for a further 4 hours. An additional heat treatment at 973 K for 4 hours was applied before the sample was oven-cooled to room temperature. X-ray diffractometry (XRD) was used to evaluate the structural properties of the prepared samples. Single phase hexagonal

compositions were found in all specimens by this method. Neutron diffraction was carried out at the time-of-flight high resolution powder diffractometer (HRPD) at ISIS, UK. This instrument has a resolution of  $\frac{\Delta d}{d}$  of  $10^{-4}$  and was used at temperatures between 4.2 and 550 K. Neutron diffraction found some traces of unreacted carbon in  $\text{Fe}_2\text{P}_{0.96}\text{C}_{0.04}$  which we here refer to as a nominal composition since the actual carbon concentration of the main phase will be somewhat smaller. Magnetic properties were measured between 10 and 400 K in a Quantum Design Physical Properties Measurement System (QD-PPMS).

#### B. Computational model

The electronic structure calculations were performed using the Vienna ab initio simulation package (VASP) code, based on DFT within projector augmented wave (PAW) method<sup>25</sup> with Perdew-Burke-Ernzerhof (PBE) parameterization<sup>26</sup>. Site-based magnetic moments were calculated using the Vosko-Wilk-Nusair interpolation<sup>27</sup> within the general gradient approximation (GGA) for the exchange-correlation potential. A  $k$ -point grid of  $11 \times 11 \times 13$  was used to discretize the first Brillouin zone and the energy convergence criterion was set  $10^{-7}$  eV during the energy minimization process. The density of states (DOS) plots presented in this work were calculated on a dense ( $19 \times 19 \times 21$ )  $k$ -grid for high accuracy. The spin-orbit interaction was turned off during the calculations and only collinear ferromagnetic (FM) and non-magnetic (NM) configurations were considered.

The minimal, nine-atom basis cell (six Fe atoms and three P atoms) was used to evaluate the total energies and magnetic properties of the alloys. Using this simple model, the effect of doping was simulated by the replacement of a single phosphorous atom by another  $p$ -block element (Z) that represents an  $x=1/3$  compositional change in the  $\text{Fe}_2\text{P}_{1-x}\text{Z}_x$  formula. Although this approach is undoubtedly oversimplified in respect of exact compositions provided in the experimental section, we believe it is still a suitable model to capture the relevant changes in the electronic structure caused by the doping elements. In order to be consistent with the experimental results, we only considered changes along the  $a$ - and  $c$ -axis by the individual expansion and compression of the  $a$ - and  $c$ -lattice parameters, without allowing any relaxation of the strained structure. In practice, we varied the lattice parameters using a stepsize of  $\pm 0.5\%$ , calculating the self-consistent electronic structures at each step.

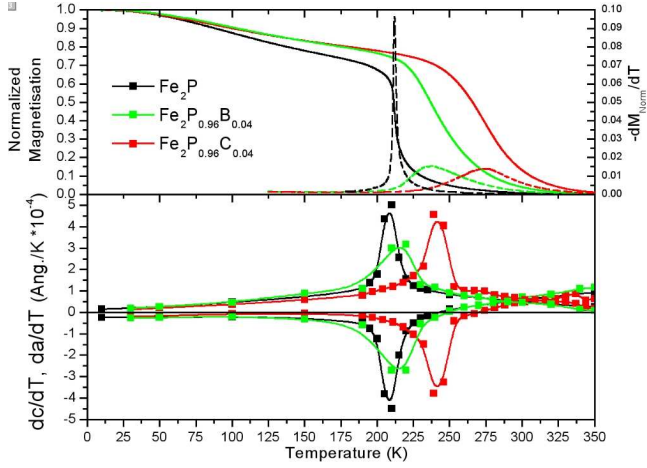


Figure 3: (Color online) Thermomagnetic curves of the parent  $\text{Fe}_2\text{P}$  alloy with the C and B doped counterparts (top, left axis) in the field of  $\mu_0 M = 0.01\text{T}$ . Derivatives ( $\frac{dM}{dT}$ ) are linked to the right axis (top). Bottom figure shows the change of the lattice parameters ( $a, c$ ) for comparison, obtained using HRPD.

## IV. RESULTS

### A. Magnetometry

The samples were first cooled to 10 K, where magnetisation curves were collected at fields up to 5 T, after which thermo-magnetic curves were collected on heating to 400 K in an applied field of 0.01 T. The results are plotted in Fig. 3. The parent alloy shows a sharp, first order transition at  $T \approx 215\text{ K}$  in accordance with values reported previously. The strong effect of doping on the magnetic order temperature is apparent. As expected, the partial replacement of P by the much smaller atomic radius B significantly increases  $T_C$ . In this study, we also partially replaced P by C atoms for the first time. The empirical atomic radius of carbon is much smaller (70 pm) than that of the phosphorus (100 pm) and boron (85 pm) elements. On the other hand, in terms of valence electrons the sequence  $\text{B}(p^1) < \text{C}(p^2) < \text{P}(p^3)$  stands. In practice, carbon doping shows a very similar effect to that of the other  $p$ -block substituents as it also clearly increases the magnetic order temperature. Furthermore, the Curie transition is heavily broadened by doping as demonstrated by the smearing out of the temperature derivative of the magnetisation ( $\frac{\partial M}{\partial T}$ ) (Fig. 3). Finally, the saturation magnetisation ( $M_S$ ) increases slightly with doping;  $M_S = 112, 113$  and  $116 \frac{\text{Am}^2}{\text{kg}}$  was obtained for  $\text{Fe}_2\text{P}$ ,  $\text{Fe}_{2.96}\text{P}_{0.04}\text{C}_{0.04}$  and  $\text{Fe}_{2.96}\text{P}_{0.04}\text{B}_{0.04}$ , respectively at 10 K in 9 T applied magnetic field. This slight increase of  $M_S$  is in line with the expectations from DFT calculations (see sec. VB). However, the samples were not fully saturated due to the large magnetocrystalline anisotropy<sup>5</sup>.

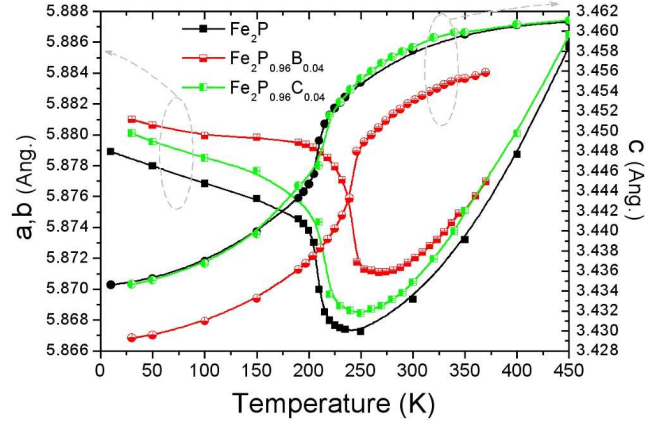


Figure 4: (Color online) Temperature evolution of the lattice parameters of the parent  $\text{Fe}_2\text{P}$  compound together with that of the C- and B-doped samples. The strong magnetoelastic response is especially apparent around the magnetic ordering temperature ( $\sim 215\text{ K}$ ).

### B. High resolution neutron diffraction

Fig. 4 shows the anisotropic lattice expansion of the  $a$ - and  $c$ -axes of  $\text{Fe}_2\text{P}$  and the doped compounds. In the magnetically ordered state ( $T \lesssim 200\text{ K}$ ) the basal plane exhibits negative lattice expansion with increasing temperature. When the temperature reaches  $T_C$ , a sharp contraction of the lattice in the  $ab$  plane is observed. The  $a$ -lattice expansion only looks Debye-like at higher temperatures ( $T \gtrsim 240\text{ K}$ ) in the paramagnetic phase. On the other hand, the thermal expansion of the  $c$ -axis is found to be positive over the entire investigated temperature range. The magnetic ordering temperature is also strongly reflected in the lattice response along  $c$ . The consequence of these counteracting lattice parameter changes over the magnetic transition is a volume change at  $T_C$  which is as small as 0.01%.

The effect of doping on the lattice parameters is clear; the basal plane of the hexagonal lattice expands whilst the  $c$ -axis shows contraction. At first glance, the anomalous thermal lattice expansion resembles that of the parent alloy. However, temperature derivatives of these quantities ( $\partial a/\partial T$ ,  $\partial c/\partial T$ ) reveal characteristic differences between the parent and doped alloys in Fig. 3. The sharpness of the derivatives demonstrates the first order nature of the magnetoelastic transition of stoichiometric  $\text{Fe}_2\text{P}$ . Although  $\partial a/\partial T$  and  $\partial c/\partial T$  are of opposite sign, they both have sharp peaks at temperature  $T_p = 209\text{ K}$ . Both B and C doping cause a shift of  $T_p$  to higher temperatures with broader  $\partial a/\partial T$  and  $\partial c/\partial T$ . These effects on the lattice properties correspond very well to the observed changes in the magnetic properties. The temperature derivative of the magnetisation in Fig. 3 (top), reveals similar broadening of the ferromagnetic transition with B or C doping.

HRPD is capable of tracking the change in the inter-



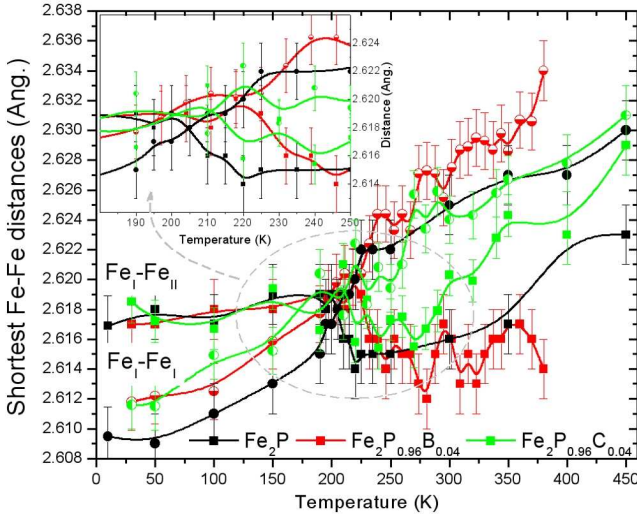


Figure 5: (Color online) The shortest  $\text{Fe}_I\text{-}2\text{Fe}_I$  and  $\text{Fe}_I\text{-}2\text{Fe}_{II}$  distances as a function of temperature for all investigated samples. Inset depicts the temperature region of the crossover.

atomic distances, thus providing vital information about the magnetoelastic coupling in these materials. The evolution of the lattice parameters through the magnetoelastic transition is already a clear indication of the significant changes of the atomic distances. Both the 3f and 3g positions of the iron atoms are low symmetry positions described by the positional parameters  $x_I$  and  $x_{II}$ , respectively. Iron atoms on the 3f-site ( $\text{Fe}_I$ ) are connected to 2 other iron atoms of the same type, denoted as  $\text{Fe}_I\text{-}2\text{Fe}_I$ . There are also two distinctive  $\text{Fe}_I\text{-}2\text{Fe}_{II}$  and  $\text{Fe}_I\text{-}4\text{Fe}_{II}$  connections to iron atoms located at the 3g-site ( $\text{Fe}_{II}$ ). Finally, there exists a relatively close  $\text{Fe}_{II}\text{-}4\text{Fe}_{II}$  distance above 3 Å. In Fig. 5, we only plot the two shortest distances,  $\text{Fe}_I\text{-}2\text{Fe}_I$  and  $\text{Fe}_I\text{-}2\text{Fe}_{II}$ , as a function of temperature, evaluated from Rietveld refinements of the HRPD data. In all of the investigated samples, the  $\text{Fe}_I\text{-}2\text{Fe}_{II}$  distance is the shortest Fe-Fe separation at low temperatures (<200 K). The latter increases with temperature, eventually becoming larger than the  $\text{Fe}_I\text{-}2\text{Fe}_I$  distance, which is strongly reduced in the vicinity of the magnetic transition temperature. The point in temperature above which  $\text{Fe}_I\text{-}2\text{Fe}_I$  is the shortest Fe-Fe distance is between 190 and 220 K for all samples.

In addition we can distinguish two groups of metal-metalloid distances:  $\text{Fe}_I\text{-}(P_I, P_{II})$  and  $\text{Fe}_{II}\text{-}(P_I, P_{II})$ . The shortest one is  $\text{Fe}_I\text{-}2P_I$ , followed by  $\text{Fe}_I\text{-}2P_{II}$ ,  $\text{Fe}_{II}\text{-}P_{II}$  and  $\text{Fe}_{II}\text{-}4P_I$ . Fig. 6 contains the two shortest distances only. The separation of  $\text{Fe}_{II}\text{-}P_{II}$  and  $\text{Fe}_{II}\text{-}4P_I$  atoms is in the range of  $\sim 2.37$  Å and  $\sim 2.49$  Å, respectively. It is worth noting that both  $\text{Fe}_I\text{-}2P_I$  and  $\text{Fe}_{II}\text{-}P_{II}$  distances only have components within the  $ab$ -plane which explains the resemblance of their temperature evolution to that of the  $a$  lattice parameter in Fig. 4: the shortest  $\text{Fe}_I\text{-}2P_I$  distance decreases sharply around the magnetic transition temperature in the parent alloy and

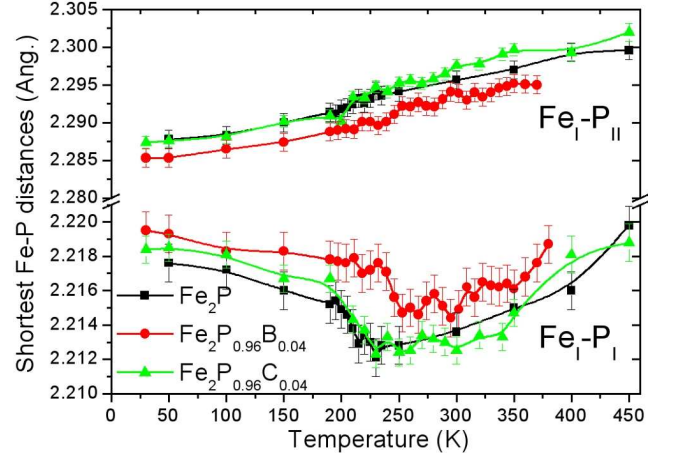


Figure 6: (Color online) The shortest metal-metalloid distances,  $\text{Fe}_I\text{-}2P_I$  and  $\text{Fe}_I\text{-}2P_{II}$  as a function of temperature in  $\text{Fe}_2\text{P}$  together with the doped counterparts. Both distances relate to the metamagnetic 3f ( $\text{Fe}_I$ ) site.

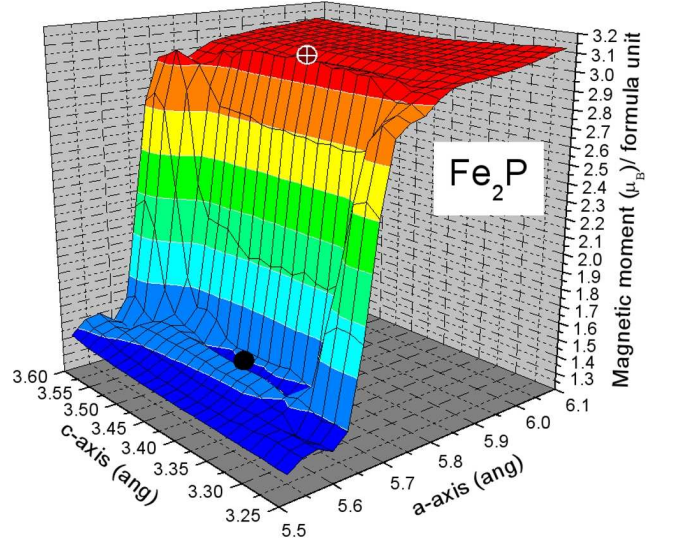


Figure 7: Total magnetisation as a function of lattice parameter of  $\text{Fe}_2\text{P}$ . Magnetisation is strongly linked to the change in  $a$ -lattice parameter.

the doped compounds. The larger  $a$  lattice parameter in the doped compounds means that the metal-metalloid distance is largest in those samples.

## V. THEORETICAL RESULTS

### A. Stoichiometric $\text{Fe}_2\text{P}$

The variation of total magnetisation with lattice parameters expected from our DFT calculations is plotted in Figure 7. A change in the lattice can have a very strong effect on the magnetic properties. The lattice expansion

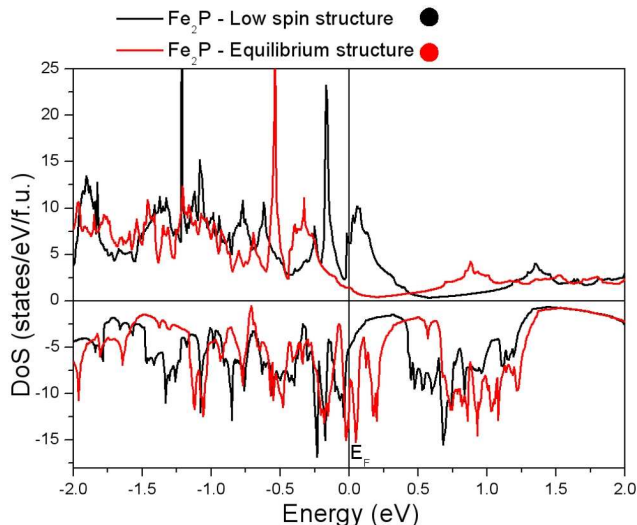


Figure 8: (Color online) Comparison of the density of states of a high magnetisation state (red) and a low magnetisation state (black) in  $\text{Fe}_2\text{P}$ .

within the basal plane causes the total magnetisation to increase abruptly from  $\sim 1.3 \mu_B$  to  $3.1 \mu_B$  around a critical value of  $a \approx 5.7 \text{ \AA}$ , and stays practically constant above it. The magnetisation varies very little with  $c$ , reflecting the greater importance of the atomic distances within the basal plane, where the atoms are packed more densely. In order to depict the changes related to the electronic structure that are most relevant to such an anisotropic magneto-elastic coupling, we compare the total electronic density of states (DOS) of the high and low magnetisation states, at  $(a, c)$  values indicated by red and black dots in Figure 7. The lattice structure in the high magnetic state has a high and sharp DOS at  $E_F$  with  $\sim 80\%$  spin polarisation, dominated by minority spins (Figure 8, red line). This signature is typical of a magnetic instability. When the lattice is compressed within the basal plane, the magnetic ground state is significantly different, as shown in black in Figure 8. The filled bands in the bottom contain the phosphorus  $3s$  states. The conduction band is formed by the  $3d$  states of Fe and the  $3p$  states of P as is typical of strong  $p$ - $d$  hybridization. The hybridized states are also present near the Fermi level, influencing the exchange splitting of the  $3d$  states of Fe. The effect of the smaller  $a$ -lattice parameter (low magnetisation state) is to reduce the exchange splitting considerably. The high peaks in the majority density of states located around  $-0.5 \text{ eV}$  are shifted to  $-0.2 \text{ eV}$ . In the minority DOS, the opposite trend is observed as the triple peak feature between  $0$  and  $0.25 \text{ eV}$  is lowered to around  $-0.25 \text{ eV}$ .

The relationship between the DOS at the Fermi Energy,  $D(E_F)$  and the strength of magnetic exchange,  $I$ , can be expressed as the Stoner criteria  $I \times D(E_F) > 1$  for an itinerant ferromagnet. Such an analysis has been extensively discussed by Eriksson et al.<sup>28</sup>. They inves-

tigated site-related magnetic stability and also found a magnetic instability with decreasing cell volume. In our study we concentrate on comparing the differences in spin densities of the high and low magnetic configurations, plotted in Fig. 9. As a consequence of the lattice symmetry, the shortest metal-metalloid distance,  $\text{Fe}_I\text{-P}_{II}$ , as well as the shortest metal-metal separation,  $\text{Fe}_I\text{-Fe}_{II}$ , have projections along both the  $a$ - and  $c$ -axes, and so this is the most suitable cross-section for our analysis.

We can ascribe three competing effects to the magnetoelastic transition. Firstly, with increasing temperature the separation between  $\text{Fe}_I$  and  $\text{Fe}_{II}$  atoms increases monotonously as observed experimentally (see Fig. 5). This is linked to our recent investigations of the exchange coupling mechanism among the magnetic sites using the exact muffin-tin orbital (EMTO) method. Our exchange coupling analysis<sup>19</sup> found that the largest contribution to the decrease in the  $c/a$  ratio to the total magnetic exchange interaction is the weakened magnetic interaction between the Fe atoms on  $3f$  and  $3g$  sites. Secondly, at the magnetic transition the  $\text{Fe}_I\text{-Fe}_I$  distance is also altered and it becomes comparably to the  $\text{Fe}_I$  and  $\text{Fe}_{II}$  but the exchange constant between these atoms is only the fraction of the  $\text{Fe}_I$  and  $\text{Fe}_{II}$  exchange, and has a less pronounced dependence on distance. Thirdly, the shortest  $\text{Fe}_I\text{-P}_I$  distance, located in the  $ab$  plane also dips around the transition temperature. This results in a significantly stronger hybridisation that can explain the decrease in magnetisation and alternation of these bonds, and hence trigger a lattice distortion in the first place. A similar scenario was also drawn from the comparison of the total electronic charge density in the FM and PM states of Mn and Si doped  $\text{Fe}_2\text{P}$ -type alloy by Dung et al.<sup>9</sup>

Our current DFT results provide further evidence for an understanding of the microscopics of the Curie transition. The calculations reveal the unusual duality of the magnetic structure of  $\text{Fe}_2\text{P}$  in which there is a large magnetic moment of  $M(\text{Fe}_{II})=2.16 \mu_B$  on the  $3g$ -site together that coexists with a significantly smaller,  $M(\text{Fe}_I)=0.85 \mu_B$ , moment on the  $3f$  crystallographic site. These findings are in full agreement with previous studies (see Sec. II). If we consider solely the effect of the structural changes that we know to occur at the Curie transition (Fig. 5), we find that there is a redistribution of magnetisation of the  $\text{Fe}_I$ -site. The large and localised magnetic moment on the  $\text{Fe}_{II}$  site is decreased in amplitude to  $\sim 1.3 \mu_B$  above the transition and strong delocalisation of the  $\text{Fe}_I$  magnetisation occurs simultaneously. Electrons from the  $\text{Fe}_I$ -site that have a magnetic contribution are redistributed along the  $c$ -axis in directions that link the  $\text{Fe}_I$  and  $\text{P}_{II}$  sites. This strong coupling between magnetism and lattice is the origin of the strong magnetoelastic response and the highly field dependent transition in these alloys. In the following section, we compare the effect of doping on the structure and magnetic properties obtained by means of DFT using structural data from neutron diffraction (HRPD).

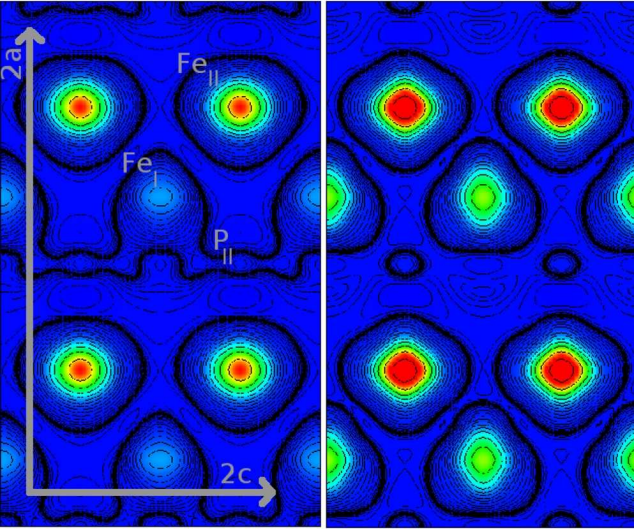


Figure 9: (Color online) A comparison of the spin density of the high magnetisation state (right) and low magnetisation state (left) of  $\text{Fe}_2\text{P}$ . The large magnetic moment around the  $\text{Fe}_{II}$  site is only decreased in amplitude above the transition, when strong delocalisation of the  $\text{Fe}_I$  magnetisation occurs simultaneously.

### B. The Effect of Doping

There exist two crystallographic sites where the metalloid elements can be incorporated into the lattice, albeit with strong site preference as described in Sec. II. Experimentally, elements with an atomic radius smaller than P were found to show a preference in the single-fold position (1b), whilst larger elements tends to occupy the twofold symmetry site (2c) in the hexagonal lattice. In order to establish the site preference from DFT calculations, we compare the difference in total energy for the different elemental substitution. First of all, the calculated total energies of the FM solutions (at any  $(a, c)$  lattice parameter value) were always found to be energetically more stable than that of the NM configurations by typically 1.5-3 eV/f.u., yielding a strong tendency toward the formation of magnetic order in all the investigated alloys. The site preference of the dopants can be established by calculating the difference in total energy ( $dE$ ) between the single-fold and two-fold site position occupancies using the equilibrium lattice of the FM state. The calculations find a clear trend with the size of the substituents: the energy difference is negative for elements that are smaller than P (left hand side of Fig. 10), reflecting the preference for singlefold occupation. On the other hand, a substituent with larger atomic radii (Si and As) prefers to occupy the twofold position of the hexagonal lattice.

This theoretically established site occupation of the dopant elements is in line with the experimental findings see Sec. II, suggesting the dominance of size effects. Therefore, we hereafter focus our magnetoelastic investigations on the effect of single-fold site occupation by the

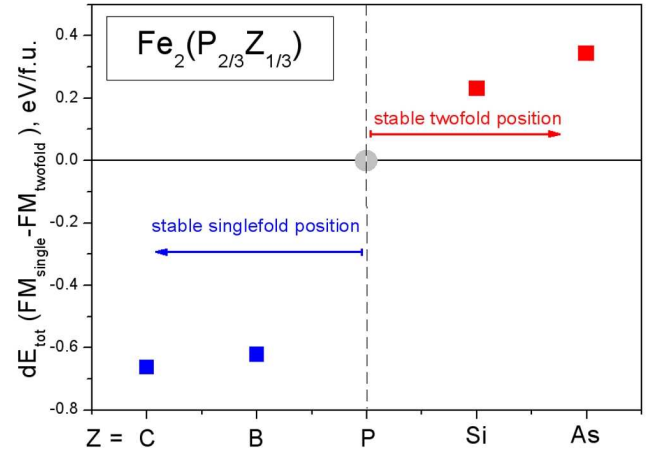


Figure 10: (Color online) Site preference of the  $p$ -block dopants as established from DFT. Negative total energy differences represent preference for the single-fold position. Positive total energy differences suggest tendency for two-fold site occupancy.

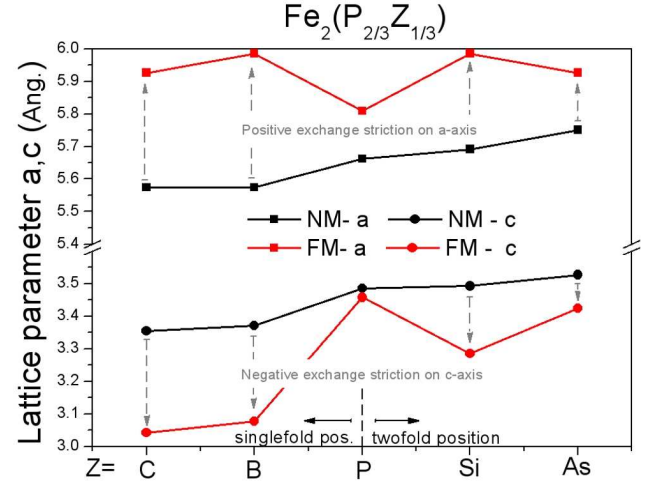


Figure 11: (Color online) Equilibrium lattice parameters for NM and FM states as a result of DFT calculations as a function of dopants in  $\text{Fe}_2\text{P}_{2/3}\text{Z}_{1/3}$ , where  $Z = \text{C, B, Si, or As}$ , respectively.

small C and B elements and the two-fold site occupation of the large Si and As elements.

The effect of doping on the lattice parameters is shown in Fig. 11. The non-magnetic (NM) calculations (black line) show an increasing trend in both the  $a$ - and  $c$  parameters of the hexagonal structure with the inclusion of larger atomic radius, anionic  $p$ -block elements. This behaviour is easily anticipated in terms of chemical pressure as the lattice is expected to adapt according to the size of dopant. Examining Fig. 11, the steepest change in the lattice is seen with the partial replacement of P by B atoms, due to the largest difference in atom size between these elements. However, in the presence of ferromagnetic (FM) interactions, any monotonic relation of lattice



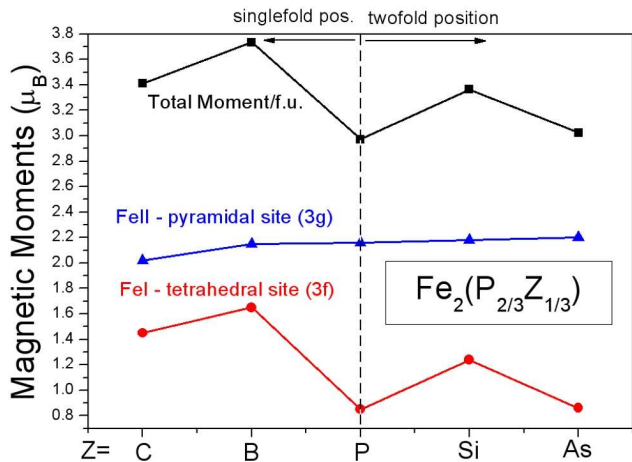


Figure 12: (Color online) Total and site-projected magnetic moments in  $\text{Fe}_2\text{P}_{2/3}\text{Z}_{1/3}$ , for  $\text{Z}=\text{C}, \text{B}, \text{Si}$  and  $\text{As}$ , respectively.

parameter to the atomic radius of the dopant is broken. The parent alloy has significantly smaller  $a$  and larger  $c$  parameters in the FM ground state than the doped compounds. The onset of ferromagnetism increases the separation of atoms within the basal plane (positive exchange striction) while their separation along the  $c$ -axis is reduced (negative exchange striction), regardless of the size or valence state of the dopant as compared to the parent composition ( $\text{Fe}_2\text{P}$ ). The overall volume change caused by the ferromagnetic exchange is positive, dominated by the larger  $a$  parameter ( $V_{hex} = a^2 c \sin(2\pi/3)$ ). Based on these calculations, one would expect the lattice to expand along the  $a$ -axis with a simultaneous contraction of the  $c$ -axis in the vicinity of the magnetic ordering temperature. Indeed, experimental (HRPD) measurements clearly reveal this sharp positive exchange striction in the basal plane and the shrinkage of the  $c$ -axis upon cooling the sample through the Curie temperature (see Fig. 4).

The significant coupling of the lattice dimensions to the magnetism also becomes apparent from the analysis of the total and site-projected magnetic moments as plotted in Fig. 12. The magnetic moment of  $\text{Fe}_{II}$  atoms show very little variation with doping and stays at around  $2.2 \mu_B$ . Although the larger  $p$ -block dopants increase the separation of the  $\text{Fe}_{II}$ - $\text{Fe}_{II}$  atoms, this distance is typically above 3 Å, and so doping only slightly alters the exchange-split states. In strong contrast, the site-resolved magnetisation of the 3f site is found to be much more sensitive to the valence electron number of the anionic elements. Examining Fig. 12 there is a strong relation between added valence electron number and magnetisation with  $\text{Z}=\text{B}$  ( $-2e^-$ ),  $\text{C}$  ( $-1e^-$ ),  $\text{P}$  ( $-$ ),  $\text{Si}$  ( $-2e^-$ ), or  $\text{As}$  ( $-$ ). This feature can be explained in terms of charge transfer from  $\text{Fe}_I$  to the anionic  $\text{Z}$  element in order to fill the electronegative  $p$  shell of the latter. The charge transfer is distance dependent and is strongly suppressed by the strong  $p$ - $d$  interaction at smaller  $\text{Fe}_I$ - $\text{Z}$  separations, while lattice expansion suppresses  $p$ - $d$  hy-

bridization and increases the degree of localisation and ionic bonding in the system. With doping, the short  $\text{Fe}_I$ - $\text{Z}$  distances are strongly influenced, altering the balance between magnetic moment formation (Fig. 9) and bond formation. The larger magnetic moments on the  $\text{Fe}_I$  atoms that result from doping account for the expansion of the basal plane as indicated by the comparison of Figs. 11 and 7.

## VI. SUMMARY AND CONCLUSION

We have used high resolution neutron diffraction (HRPD) as well as density functional theory to investigate the effect of  $p$ -block elements doping on the magnetoelastic properties of  $\text{Fe}_2\text{P}$ . HRPD has revealed that the strong coupling between the magnetism and the lattice is manifested by the contraction of the basal plane and by a significant increase of the  $c$ -axis on heating through the magnetic transition, resulting in a small overall volume change of the lattice ( $>0.01\%$ ). A simultaneous change in both the metal-metal and metal-metalloid distances is observed.

DFT calculations reveal that the magnetic properties are strongly dependent on expansion in the basal ( $ab$ ) plane, while they are almost invariant with regard to variation of the  $c$  parameter. The strong dependence of magnetic moments on the 3f site is related to the  $a$  lattice parameter being on the verge of a metamagnetic transition. The closest metal-metal and metal-metalloid distances - the latter ones also linked to the metamagnetic 3f site - are strongly altered by both the  $d$ - $d$  and  $p$ - $d$  hybridisation energies at the transition. As a result, the redistribution (delocalisation) of the magnetisation from the 3f site along the  $\text{Fe}_I$ - $\text{P}_{II}$  chains in the  $c$ -axis direction occurs as shown in Fig. 9, implying its strong influence on bonding (also suggested by Dung et al.<sup>10</sup>). The magnetic moment on the 3g site is only slightly reduced (to  $\sim 1.3 \mu_B$ ) above the transition, accounting for the observed strong divergence of the Curie-Weiss law<sup>5</sup>.

Our theoretical investigations on the effect of doping show that elements with an atomic radius smaller than phosphorus (e.g.  $\text{C}$  or  $\text{B}$ ) occupy single-fold (1b) sites while larger elements such as  $\text{Si}$  or  $\text{As}$  prefer to occupy the two-fold symmetry site (2c) in the hexagonal lattice. The magnetism on the high magnetic site (3g) is not influenced by the dopant and stays approximately constant ( $\sim 2.2 \mu_B$ ). By contrast, the iron atoms on the metamagnetic site develop larger magnetic moments, in direct relation to the valence electron number of the doping element. As a result, the conditions for the metamagnetic transition of the 3f site are locally modified, resulting in a smearing of the transition as observed experimentally. Indeed, the larger exchange splitting on  $\text{Fe}_I$  results in increased exchange coupling parameters, significantly increasing the Curie temperature<sup>19</sup>.

The large difference in the lattice equilibrium between the non-magnetic and ferromagnetic solutions in the par-



ent compound as well as in the doped materials as found by DFT calculations suggests that the magnetic properties are not only very sensitive to compositional inhomogeneities but also to internal strains set by the preparation conditions<sup>29</sup>. Therefore for applications (such as magnetic refrigeration), where the transition temperature needs to be set by the material to a high accuracy, elements such as Si and As are favorable but process control will be crucial. Finally, as the remarkable change in magnetic ordering of these alloys is linked to the lattice parameters within the basal plane, uniaxial thin films on flexible substrates could be exploited to electrically manipulate the magnetic properties of this material system.

## Acknowledgments

We thank L. Szunyogh for useful discussions and D. Boldrin for help with sample preparation. We also thank K.S. Knight for providing us with the <sup>11</sup>B isotope used for this study. Financial support is acknowledged from The Royal Society (KGS) and EPSRC grant EP/G060940/1 (KGS and ZG). Fig. 9 was prepared using VESTA open-source software.<sup>30</sup> Computing resources provided by Darwin HPC and Camgrid facilities at The University of Cambridge and the HPC Service at Imperial College London are gratefully acknowledged.

- 
- <sup>1</sup> P. Dera, B. Lavina, L. A. Borkowski, V. B. Prakapenka, S. R. Sutton, M. L. Rivers, R. T. Downs, N. Z. Boctor, and C. T. Prewitt, *Geophys. Res. Lett.* **35**, L10301 (2008).
  - <sup>2</sup> H. P. Scott, B. Kiefer, C. D. Martin, N. Boateng, M. R. Frank, and Y. Meng, *High Pressure Research* **28**, 375 (2008).
  - <sup>3</sup> P. S. Herle, B. Ellis, N. Coombs, and L. F. Nazar, *Nat. Mater.* **3**, 147 (2004).
  - <sup>4</sup> J. Wang, Q. Yang, J. Zhou, K. Sun, Z. Zhang, X. Feng, and T. Li, *Nano Research* **3**, 211 (2010).
  - <sup>5</sup> H. Fujii, T. Hōkabe, T. Kamigaichi, and T. Okamoto, *Journal of the Physical Society of Japan* **43**, 41 (1977).
  - <sup>6</sup> R. J. A. A. Catalano and A. Wold, *J. Solid State Chem.* **262**, 313 (1973).
  - <sup>7</sup> T. E. L. H. C. W. R. Chandra, S. Bjarman and R. Wappling, *J. Solid State Chem.* **34**, 389 (1980).
  - <sup>8</sup> L. H. P. Jernberg, A. A. Yousif and Y. Andersson, *J. Solid State Chem.* **53**, 313 (1984).
  - <sup>9</sup> N. H. Dung, Z. Q. Ou, L. Caron, L. Zhang, D. T. C. Thanh, G. A. de Wijs, R. A. de Groot, K. H. J. Buschow, and E. BrÅEck, *Advanced Energy Materials* **1**, 1215 (2011), ISSN 1614-6840.
  - <sup>10</sup> N. H. Dung, L. Zhang, Z. Q. Ou, L. Zhao, L. van Eijck, A. M. Mulders, M. Avdeev, E. Suard, N. H. van Dijk, and E. Brück, *Phys. Rev. B* **86**, 045134 (2012).
  - <sup>11</sup> M. D. Kuz'min and M. Richter, *Phys. Rev. B* **76**, 092401 (2007).
  - <sup>12</sup> A. Fujita, Y. Akamatsu, and K. Fukamichi, *Journal of Applied Physics* **85**, 4756 (1999).
  - <sup>13</sup> A. Fujita and H. Yako, *Scripta Materialia* **67**, 578 (2012), ISSN 1359-6462.
  - <sup>14</sup> K. G. Sandeman, *Scripta Mater.* **67**, 566 (2012).
  - <sup>15</sup> H. Yamada and K. Terao, *Phase Transitions* **75**, 231 (2002).
  - <sup>16</sup> E. K. Delczeg-Czirjak, L. Bergqvist, O. Eriksson, Z. Gercsi, P. Nordblad, L. Szunyogh, B. Johansson, and L. Vitos, *Phys. Rev. B* **86**, 045126 (2012).
  - <sup>17</sup> L. Severin, L. Haggstrom, L. Nordstrom, Y. Andersson, and B. Johansson, *Journal of Physics: Condensed Matter* **7**, 185 (1995).
  - <sup>18</sup> E. K. Delczeg-Czirjak, L. Delczeg, M. P. J. Punkkinen, B. Johansson, O. Eriksson, and L. Vitos, *Phys. Rev. B* **82**, 085103 (2010).
  - <sup>19</sup> E. K. Delczeg-Czirjak, Z. Gercsi, L. Bergqvist, O. Eriksson, L. Szunyogh, P. Nordblad, B. Johansson, and L. Vitos, *Phys. Rev. B* **85**, 224435 (2012).
  - <sup>20</sup> A. Barcza, Z. Gercsi, K. S. Knight, and K. G. Sandeman, *Phys. Rev. Lett.* **104**, 247202 (2010).
  - <sup>21</sup> Z. Gercsi, K. Hono, and K. G. Sandeman, *Phys. Rev. B* **83**, 174403 (2011).
  - <sup>22</sup> Z. Gercsi and K. G. Sandeman, *Phys. Rev. B* **81**, 224426 (2010).
  - <sup>23</sup> J. B. Staunton and B. L. Gyorffy, *Phys. Rev. Lett.* **69**, 371 (1992).
  - <sup>24</sup> H. Fujii, S. Komura, T. Takeda, T. Okamoto, Y. Ito, and J. Akimitsu, *Journal of the Physical Society of Japan* **46**, 1616 (1979).
  - <sup>25</sup> G. Kresse and J. Furthmuller, *Phys. Rev. B* **54**, 11169 (1996).
  - <sup>26</sup> J. P. Perdew, K. Burke, and M. Ernzerhof, *Phys. Rev. Lett.* **77**, 3865 (1996).
  - <sup>27</sup> S. H. Vosko, L. Wilk, and M. Nusair, *Canadian Journal of Physics* **58**, 1200 (1980).
  - <sup>28</sup> B. J. L. H. O. Eriksson, J. Sjostrom and H. L. Skriver, *J. Magn. Magn. Mater.* **74**, 347 (1988).
  - <sup>29</sup> Z. Gercsi and M. Hudl, Quenched samples from the annealing temperature show significantly different magnetic properties as compared to oven cooled ones. Private communication.
  - <sup>30</sup> K. Momma and F. Izumi, *Journal of Applied Crystallography* **41**, 653 (2008).